J Mater Sci (2017) 52:815–831

Improved lithium adsorption in boron- and nitrogen-substituted graphene derivatives

Murugan Lalitha[1], Shivaraja Selva Mahadevan[1], and Senthilkumar Lakshmipathi[1,*]

[1] *Department of Physics, Bharathiar University, Coimbatore, Tamil Nadu 641046, India*

Received: 8 July 2016
Accepted: 6 September 2016
Published online: 16 September 2016

ABSTRACT

We present the results from density functional theory calculations of the lithium adsorption on various forms of boron- and nitrogen-doped graphene derivatives. Encouraging results are noticed for the lithium adsorption on the boron-doped graphyne model. The acetylenic linkage increases the lithium adsorption affinity but decreases the gravimetric densities marginally in bare, boron/nitrogen-doped graphene derivatives. From lithiation potential, gravimetric density, and specific capacity values, we notice boronated graphyne as a highly suitable anode material for Li-ion batteries.

Introduction

Growing global energy demand requires the development of high-efficiency energy storage systems [1, 2]. Presently, electrochemical systems such as batteries and supercapacitors are the reliable energy storage systems due to their high specific energy, high efficiency, and long life [3]. Commercially, lithium-ion batteries made a renaissance in the energy storage systems, as they offer several advantages such as rechargeability, high energy density, and longer lifespan [4]. To improve the performance of lithium batteries, breakthroughs are constantly accomplished through the improvement in electrode and electrolyte components [5]. Traditionally, lithium transition metal oxides ($LiCoO_2$, $LiNiO_2$, and $LiMgO_2$), layered metal oxides (V_2O_5), and chalcogenides (TiS_2) are highly favorable for cathode materials [6–10], while graphite and silicon are the widely used commercial anode materials in the battery technology [11]. However, both graphite and silicon are not ideal anode materials since graphite has a limited storage capacity of 372 mAh/g [12], while silicon has the very limited cycle life [13]. Nevertheless, studies on low-dimensional materials [14–16] such as graphene, carbon nanotubes, and fullerenes have shown prospects for the use of potential anode materials in lithium-ion batteries [17] due to their large surface area and unique physical and chemical properties. Transition metal-decorated carbon materials [18, 19] are extensively used for the efficient hydrogen and lithium storage due to the presence of ionic site rather than the van der Waals surface. However, the large cohesive energy of transition metals and their low interaction energy with carbon cause transition metal clustering, which hinders the storage efficiency [20–22]. Ever since its discovery in 2004 [23], two-dimensional graphene has found significant attraction in energy storage systems

Address correspondence to E-mail: lsenthilkumar@buc.edu.in

DOI 10.1007/s10853-016-0378-6

because of its excellent electrical and thermal conductivity, high charge carrier mobility, two-dimensional structure, and a broad electrochemical window [24, 25]. The adsorption of lithium atoms on graphene [26] is particularly important for various applications such as hydrogen storage, Li-ion batteries, and supercapacitors [27–30]. Besides graphene, there is a more potential interest growing toward applying the derivatives of graphene such as graphyne and graphdiyne in the areas like lithium and hydrogen storage [31, 32]. These allotropes contain a network of *sp* and sp^2 hybridized carbon atoms and have the same symmetry as graphene. For example, infinite 2D periodic sheet of graphyne is formed via three C6 hexagonal rings interconnected by three acetylenic units (–C≡C–). However, in graphdiyne the three 6C hexagonal rings are interconnected by six acetylenic units (–C≡C–), which makes it more stable than graphyne. Further, the larger surface area and various numbers of adsorption sites in addition to the bigger cavities are the attractive features of graphyne and graphdiyne than graphene, which offer a better hope for lithium storage. Studies have shown that both graphyne and graphdiyne can hold a large amount of lithium atoms with considerably higher specific capacities [31, 32]. Zhang et al. reported based on the first-principles calculations of both in-plane and out-of-plane diffusion of lithium atoms on graphyne layers the efficient intercalation density of LiC_4 [33]. Further, Chandra Shekar et al. [34] observed the rattling motion of lithium ion through the model compounds of graphyne and graphdiyne, as the diffusion of Li^+ is barrierless. All the above facts suggest that the graphyne and graphdiyne could serve as a better lithium storage material.

Doping of carbon nanostructures with boron and nitrogen atoms provides scope for improving the lithium storage, due to their equivalent atomic size in comparison with carbon. Earlier studies reported that the boron [35, 36]- and nitrogen [37]-doped graphene have higher lithium storage capability rather than its bare counterpart, confirmed both experimentally [38] and theoretically [39]. Likewise, Lu et al. [40] reported that boron-doped graphyne outperformed the undoped graphyne for both Li and H_2 storage. Besides, Ma et al. [37] explored N-doped graphene nanosheets using first-principles calculations and recommended using pyridinic N-doped graphene as an anode material for lithium battery applications. The above studies suggest the significance of boron and nitrogen atoms as dopants for lithium storage.

In the present study, the two-dimensional graphene and its allotropes such as graphyne and graphdiyne with varying acetylenic linkages (named as G422 and G442) are considered, with a view to characterize the maximum adsorption capacity of lithium atoms. It is worth to mention here that the influence of varying acetylenic chain length on the lithium adsorption capacity in the model compounds of graphyne and graphdiyne is yet to be investigated. Furthermore, the effectiveness of trivalent boron atoms and pentavalent nitrogen atoms as dopants in the model compounds for improved lithium storage is elucidated. On the whole, the results of the study will be useful for using graphene derivatives as efficient lithium storage materials and possibly alternative anode for lithium batteries.

Methodology

The two-dimensional graphene (24 carbon atoms) and its derivative model compounds such as graphyne and graphdiyne with varying acetylenic linkages (named as G422 and G442, where 422 and 442 represent the number of carbon atoms linking the hexagonal rings in each of the three sides of the structures) are studied with a focus on enhancing the lithium adsorption capacity. Further, the graphene and its derivatives are functionalized along its unsaturated edges with 12 hydrogen atoms. Consequently, the proposed structures possess varying number of carbon atoms in graphene ($C_{24}H_{12}$), graphyne ($C_{24}H_{12}$), graphdiyne ($C_{30}H_{12}$), G442 ($C_{28}H_{12}$), and G422 ($C_{26}H_{12}$). Graphdiyne consists of the highest number of carbon atoms. Among the five graphene derivatives, G442 and G422 structures are more attractive due to the nonsymmetric acetylenic chain length along the three sides of the structure, unlike graphyne and graphdiyne. Further, to enhance lithium adsorption efficiency in graphene, graphyne, graphdiyne, G422, and G442 structures, we have doped the structures with trivalent boron atom and pentavalent nitrogen atom in one of the sp^2 hybridized carbon atoms of the hexagon site. Elemental substitution of carbon is endothermic [39] and each aromatic ring can be doped at the maximum of three atoms, and here we prefer one dopant atom per

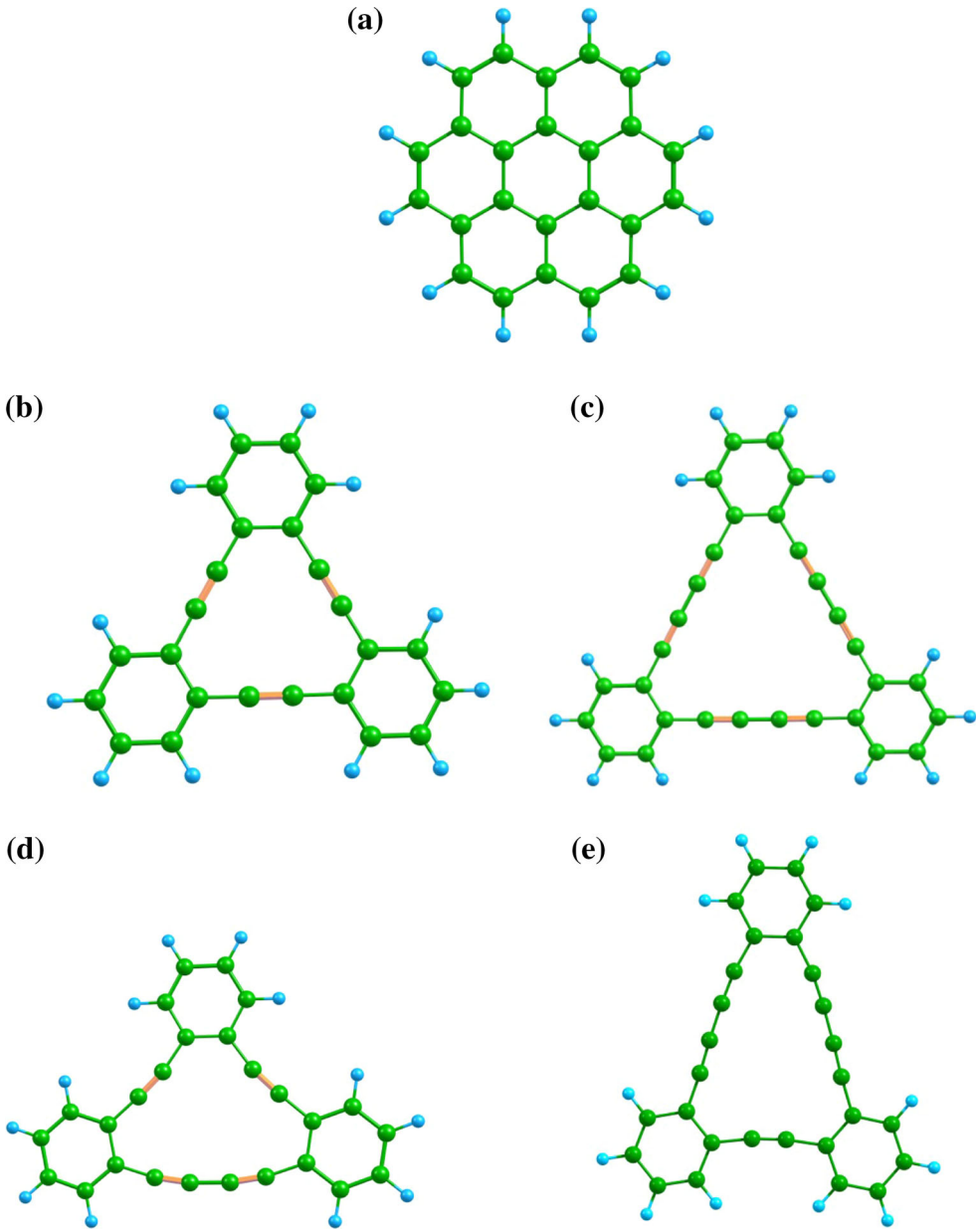

Figure 1 Optimized geometry of **a** graphene, **b** graphyne, **c** graphdiyne, **d** G422, and **e** G442. *Green balls* and *blue balls* represent carbon and hydrogen atoms, respectively.

aromatic ring. Thus, each hexagon ring of a structure contains a dopant atom, and in total three dopant atoms exist in a structure systematically. In the case of graphene, a dopant atom substitutes a single carbon atom. Subsequently, we have a variety of carbon structures to compare relative lithium adsorption efficiency. On these carbon structures, lithium atom is adsorbed sequentially increasing from 1 to 6 in order to characterize its adsorption affinity. The maximum number of lithium atoms adsorbed by a material determines its adsorption affinity.

In order to give a numerical account of the stability of the doped nanostructures, cohesive energy of the boron- and nitrogen-doped graphene framework was calculated by the following equation:

$$E_{\mathrm{coh}} = E_{\mathrm{bare}} + nE_{\mathrm{dop}} - nE_{\mathrm{carbon}} - E_{\mathrm{complex}}, \quad (1)$$

where E_{bare} is the energy of the bare structures (undoped), E_{dop} is the energy of an isolated doping atom (boron or nitrogen), n represents the number of doping atoms, E_{carbon} is the energy of an isolated carbon atom, and E_{complex} is the energy of the doped complex. Further, the adsorption energy (E_{ad}) of lithium atom on the lithiated structure is defined as follows:

$$E_{\mathrm{ad}} = E_{\mathrm{li-comp}} - (n\,E_{\mathrm{li}} + E_{\mathrm{bare}}), \quad (2)$$

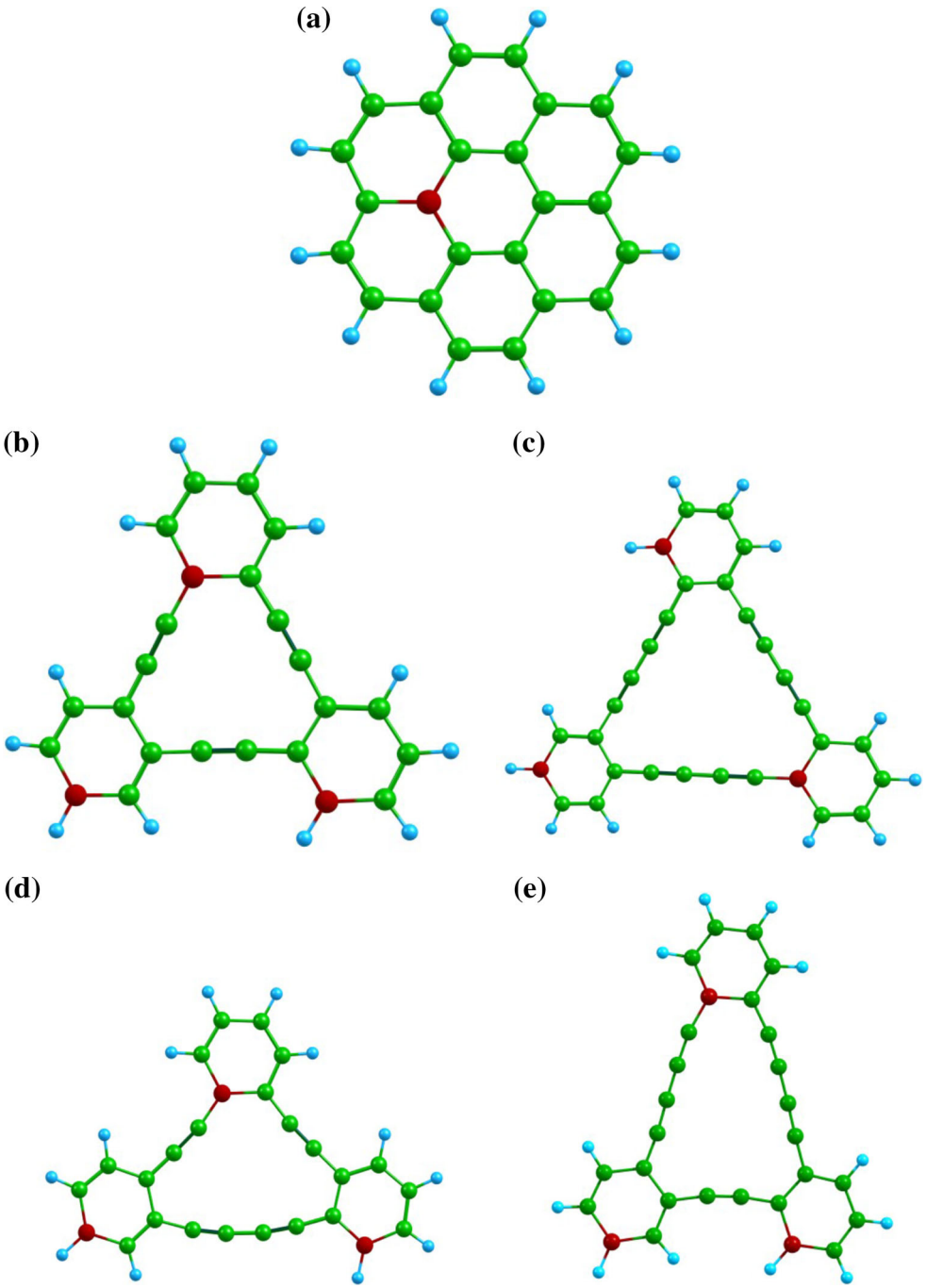

Figure 2 Optimized geometry of boron-doped **a** graphene, **b** graphyne, **c** graphdiyne, **d** G422, and **e** G442. *Maroon balls* represent boron atoms.

where E_{bare} is the energy of bare structure in the absence of lithium atoms, n is the number of lithium atoms adsorbed, E_{li} is the energy of an isolated lithium atom, and $E_{li\text{-}comp}$ is the energy of the lithiated complex.

Further, to ascertain whether these carbon allotropes are good anode materials for lithium batteries, we have calculated the lithiation potential for lithium-dispersed allotropes, specific capacity and weight percent of the lithiated complex, and the adsorption energy of lithium atom. The lithiation potential [31, 41] is determined by the following relation:

$$V = \frac{-\Delta E}{z}, \tag{3}$$

where ΔE is the adsorption energy of lithium atoms on graphene derivatives (given in eV) and z is the

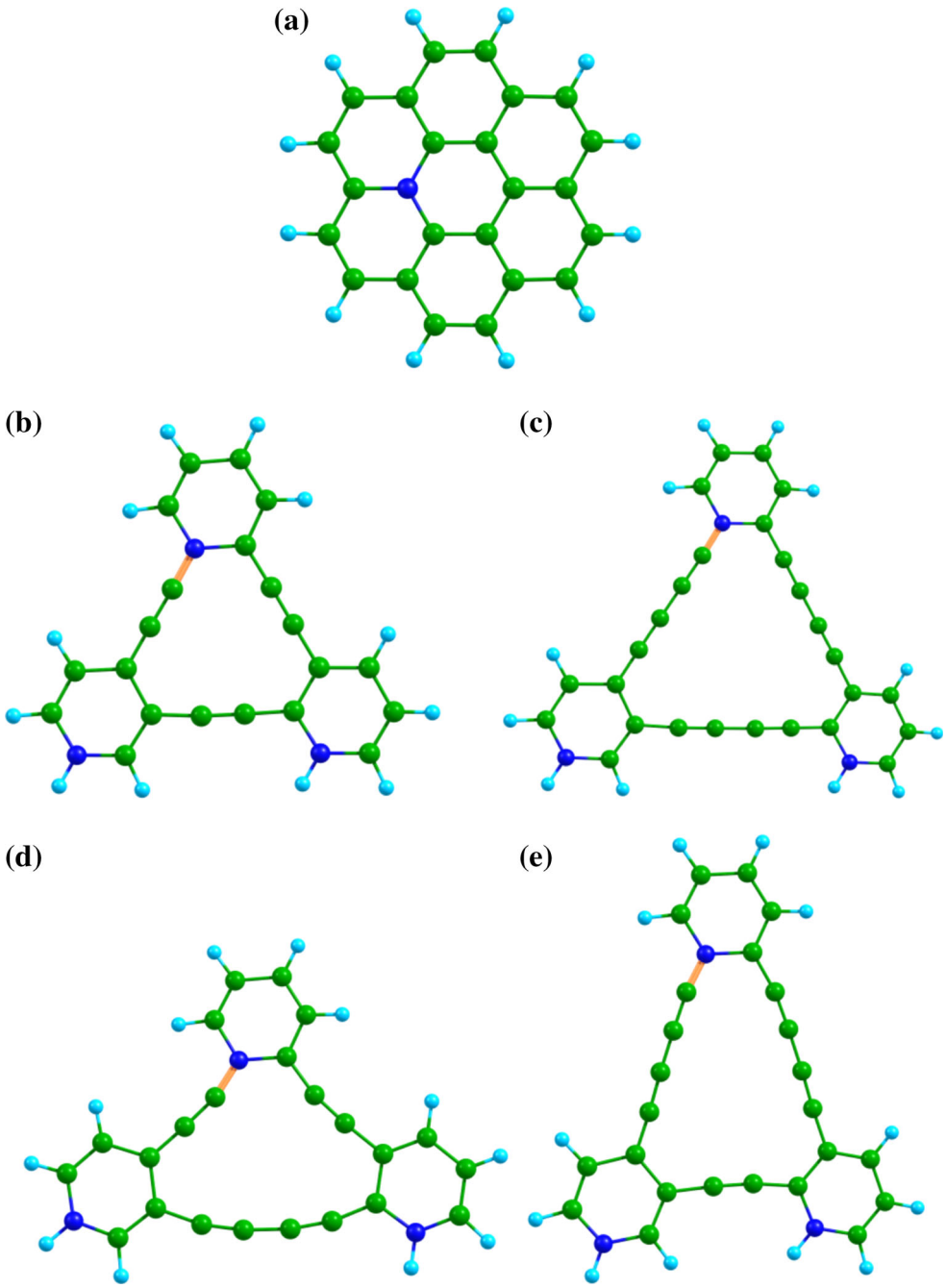

Figure 3 Optimized geometry of nitrogen-doped **a** graphene, **b** graphyne, **c** graphdiyne, **d** G422, and **e** G442. *Dark blue balls* represent nitrogen atoms.

number of lithium atoms adsorbed. The amount of charge per unit weight that a battery electrode material contains is often expressed using specific capacity (mAh/g), which defines the storage capacity, and is calculated by

$$C_{\mathrm{p}} = \frac{F}{W}, \tag{4}$$

where F is the Faraday constant (96,500 C/mol) and W is the molecular mass of the lithiated complex. The gravimetric density of the lithium atoms adsorbed is calculated by

$$W = \frac{M_{\mathrm{Li}}}{M_{\mathrm{Li}} + M_{\mathrm{sup\,port}}}, \tag{5}$$

where M_{Li} is the mass of a single lithium atom and $M_{\mathrm{sup\,port}}$ is the mass of the lithiated carbon nanostructures.

The considered graphene derivatives, its corresponding boron- and nitrogen-doped derivatives,

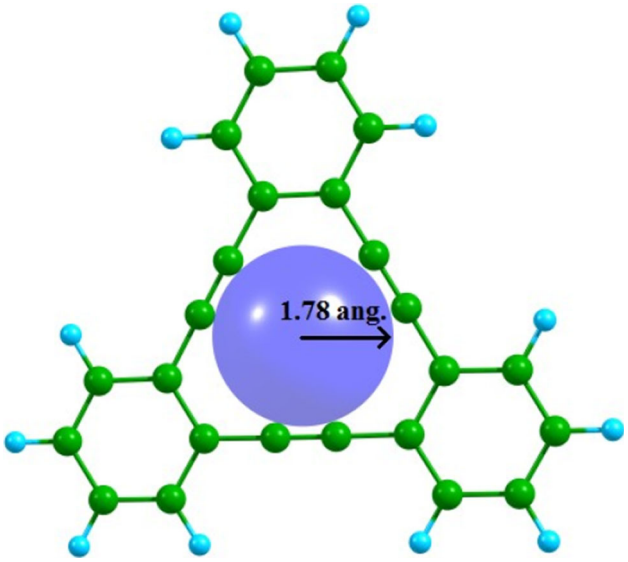

Figure 4 Illustration of the measurement of pore radius by fitting a sphere inside the cavity.

and lithium-adsorbed complexes were optimized at ωB97XD/6-311G** level of theory. ωB97XD [42] is a long-range functional widely used in dispersion-corrected DFT (DFT-D) method, while 6-311G** is commonly used for physisorption in carbon nanomaterials [43] and the study of weak intermolecular interactions [44–47], and is therefore well suited for the present study. Frequency calculations are carried out for all the structures to confirm their minima. All the calculations are carried out using Gaussian 09 [48]. Energy decomposition analysis (EDA) is performed using Amsterdam density functional theory (ADF) package [49, 50].

Results and discussion

Pore radius

The optimized geometry of graphene, graphyne, graphdiyne, G442, and G422 is displayed in Fig. 1, while the boron- and nitrogen-doped graphene derivatives are displayed in Figs. 2 and 3, respectively. Cavity size or pore radius in the graphene derivatives has a significant effect on the adsorption properties [51] and hence is measured through the maximum radius of the sphere that can fit into the pore as illustrated in Fig. 4.

The measured pore radius of bare, boron-, and nitrogen-doped carbon nanostructures are listed in Table 1, wherein the graphdiyne possesses the maximum pore radius among the structures considered due to the presence of more number of acetylenic linkages. G442 and G422 structures follow graphdiyne in pore radius order due to the decreasing number of acetylenic linkages present in the structure. Graphyne and graphene take the last two positions, respectively, in the pore radius order.

Table 1 Pore radius of bare, boron-, and nitrogen-doped structures of graphene and its derivatives

Structures	Pore radius (Å)		
	Bare structures	Boron doped	Nitrogen doped
GR	1.14	1.16	1.13
GY	1.78	1.80	1.77
GDY	2.55	2.55	2.53
G442	1.95	1.95	1.93
G422	1.93	1.94	1.91

The pore radius order of the considered nanostructures is as follows:

GDY > G442 > G422 > GY > GR.

Interestingly, on doping with boron the pore radius of the nanostructures increases but decreases with nitrogen doping possibly due to the large atomic radius and the electronegative nature of the nitrogen atom. In addition, the bond length of B–C bond (ranges between 1.50 and 1.55 Å) and the N–C bond length (ranges between 1.37 and 1.42 Å), which might have influenced the pore size. This increase in cavity size of the boron-doped carbon nanostructures will aid in the facile passage of lithium atoms, which in turn will enhance the adsorption affinity.

Cohesive energy

The stability of the boron- and nitrogen-doped systems is crucial for application purpose and hence is assessed through the cohesive energy, calculated (for a single boron and a single nitrogen atom) using Eq. 1 and listed in Table 2.

Generally, the large value of the cohesive energy indicates the higher stability of the system. Henceforth, here the boron-doped nanostructures exhibit higher magnitude (in the order of ~4 eV) of cohesive energy compared to the nitrogen-doped structures, which indicates that boron-doped derivatives are more stable than their nitrogen counterparts. Numerically, the cohesive energy of boron-doped

derivatives is 1.7 eV greater than the nitrogen-doped derivatives. Increased cohesive energy indicates the greater structural stability; hence, the boron-doped derivatives possess slightly higher stability than the nitrogen-doped derivatives. Nevertheless, both boron and nitrogen doping are equally feasible, based on their comparable cohesive energies.

Table 2 Cohesive energy for a single boron and a single nitrogen atom in graphene derivatives

Structures	Cohesive energy (eV)	
	Boron-doped complex	Nitrogen-doped complex
GR	−4.88	−3.11
GY	−4.52	−2.76
GDY	−4.45	−2.83
G442	−4.54	−2.81
G422	−4.59	−2.81

The chemical nature of boron and nitrogen dopant atoms in graphene and its derivatives strongly influences its electronic properties [52]. The electronic structures of boron- and nitrogen-doped graphene derivatives are explored through total density of states (TDOS) analysis and are compared with those of the bare graphene derivatives. The TDOS plots for the graphene derivatives are obtained using Multiwfn programs [53] and shown in Fig. 5.

From the figures, two short peaks appear in the vicinity of the Fermi energy for both boron and nitrogen doping in graphyne, graphdiyne, G442, and G422 structures. Among them, the peak corresponding to boron-doped structures shifts to the low-lying LUMO region, whereas for the nitrogen-doped

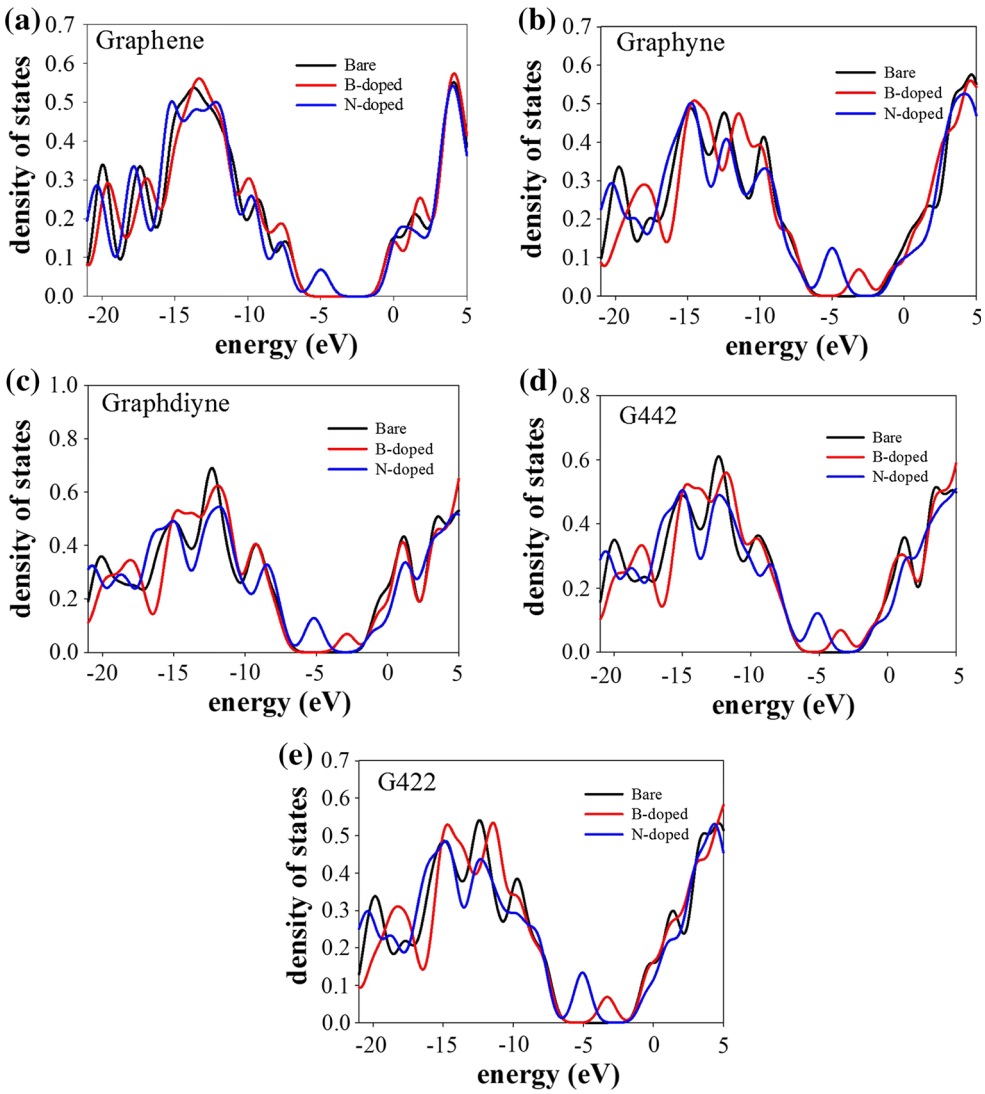

Figure 5 TDOS plots for the bare, boron-, and nitrogen-doped derivatives of **a** graphene, **b** graphyne, **c** graphdiyne, **d** G442 and **e** G422.

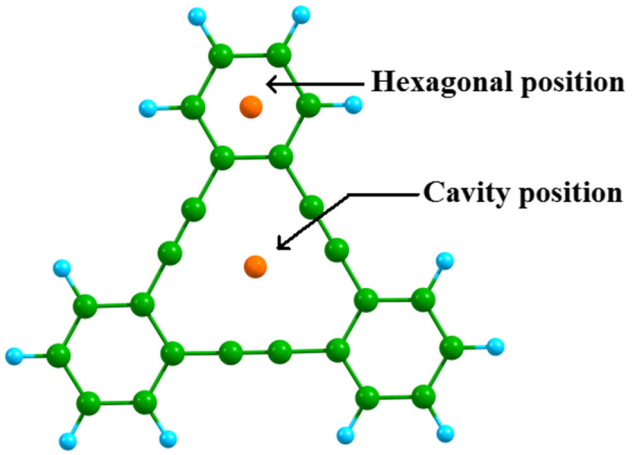

Figure 6 Illustration of the adsorption sites such as cavity position and the hexagonal position in graphyne.

structures, the peak shifts to the HOMO region. The respective shifting of the peaks near the Fermi energy toward LUMO and HOMO regions for boron and nitrogen doping corresponds to the p-type and n-type behavior of the material, respectively. In the case of graphene, boron doping does not affect the electronic properties, whereas nitrogen doping causes the n-type behavior of the graphene derivatives. Thus, both the boron and nitrogen doping induce p-type and n-type behavior of the material, respectively, which in turn aids for enhanced adsorption.

Lithium adsorption energy

We have increased the concentration of lithium atom on carbon nanostructures sequentially from 1 to 6 and optimized each case.

The adsorption of lithium on the graphene derivatives occurs at two positions, namely at the cavity position and above/below the hexagon ring of the nanostructure as illustrated in Fig. 6.

It is important to note that the lithiation is performed initially on the top, followed by the bottom surface of the considered graphene derivatives. Exclusively, in the boron-doped derivatives, up to eight atoms are lithiated, whereas up to six atoms are lithiated in nitrogen-doped derivatives, and their optimized geometries are shown in Figs. 7 and 8, respectively. The adsorption energy of monolithium atom on various adsorption sites such as cavity and hexagonal sites on graphyne, graphdiyne, G422, and G442 is given in Table 3.

In graphyne, the maximum adsorption energy of −1.72 eV is observed for lithium atom at cavity site, indicating the highest affinity toward cavity site rather than the hexagonal site. Likewise, the higher affinity toward cavity site persists on both boron- and nitrogen-doped graphene derivatives. The same trend follows also in graphdiyne, G442, and G422 structures. Despite the above, a case of contradiction is observed in GDY-B where hexagonal site shows strong affinity toward Li atom than cavity site. This is due to the larger magnitude of attractive energy terms due to higher electrostatic potential in hexagon site obtained from EDA (EDA Table S6 in supporting information) and visualized in the MESP [54, 55] (molecular electrostatic potential map in Fig. S1 supporting information). Overall, the cavity site is having more affinity toward lithium adsorption due to the reduced electron density region.

The binding energy of monolithium atom (Eq. 2) among the five graphene derivatives is given in Table S1, wherein we note that G442 offers higher adsorption energy of −0.96 eV, while graphene offers the least adsorption strength (−0.37 eV), which is consistent with the binding energy of lithium atom on graphene (0.13 eV) as calculated by Ferre-Vilaplana [56]. However, doped graphene derivatives show improved monolithium adsorption. Specifically, boron-doped structures like graphyne and G422 show marginally higher monolithium binding affinity. For systems with more than one lithium atom, the adsorption energy of lithium is calculated using Eq. 2 and is listed in supporting information (SI) Table S1. The variation of the adsorption energy of Li on the bare, boron-, and nitrogen-doped graphene derivatives with respect to the change in the number of lithium atoms is plotted in Fig. 9.

From this figure, the enhanced lithium adsorption is observed for boron doping in graphene and all of its derivatives. The reason behind this is that boron doping transforms the graphene derivatives to an electron-deficient system, which increases the electronic conductivity and subsequently enhances the adsorption affinity. Likewise, the adsorption of lithium in nitrogen-doped graphene derivatives is improved compared to bare graphene derivatives, although being weaker in magnitude than the boron-doped derivatives due to the electron-rich nature of the nitrogen atoms. As a case of exception, bare G442 complex shows better lithium adsorption efficiency than its nitrogen counterpart. The increasing nature of the

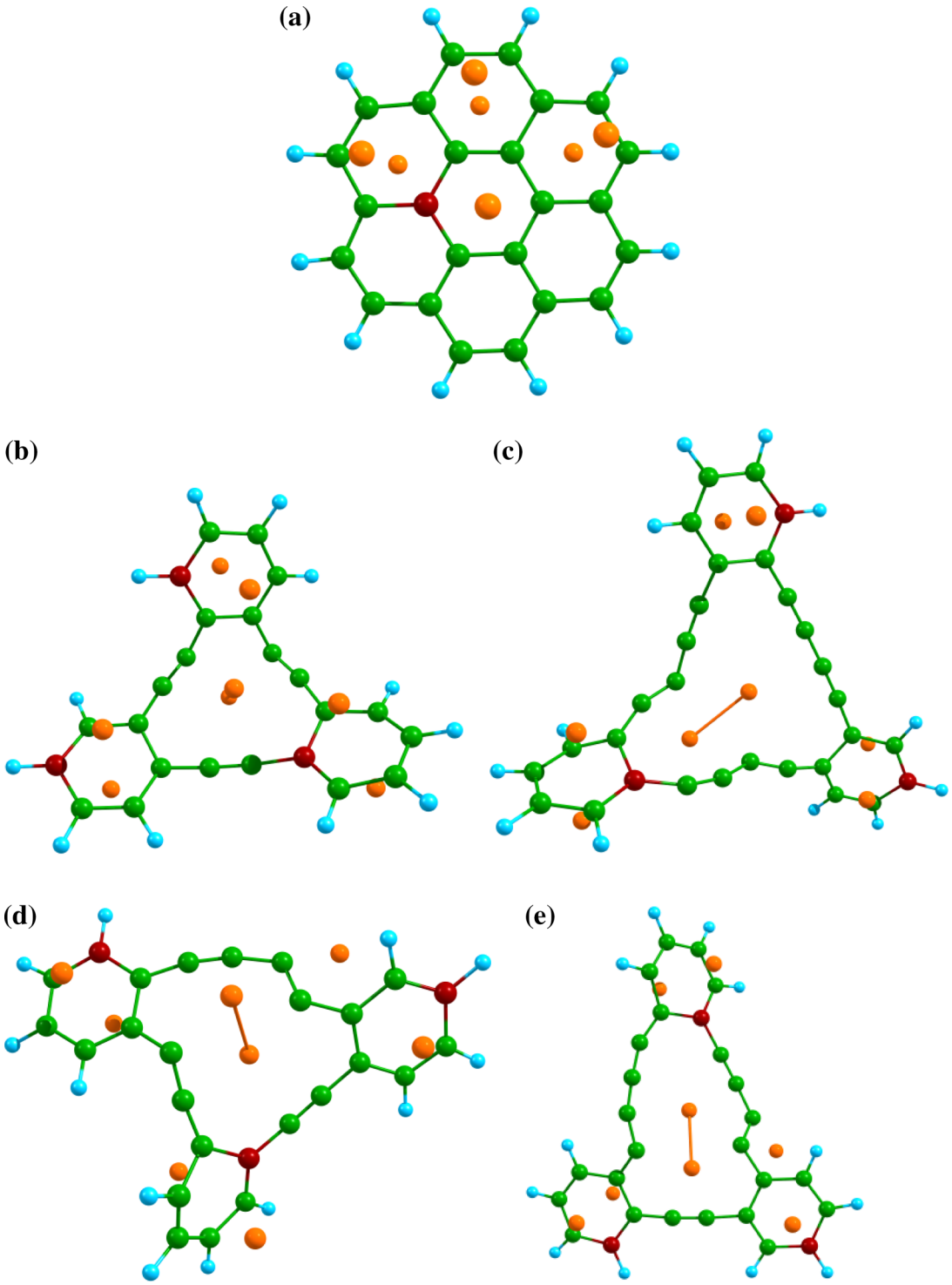

Figure 7 Optimized geometry of eight lithium atoms adsorbed on boron-doped **a** graphene, **b** graphyne, **c** graphdiyne, **d** G422, **e** G442. *Orange balls* represent lithium atoms.

adsorption energy curve is due to the cumulative effect of the adsorption of the lithium atoms. However, we speculate that the adsorption energy/Li curve will saturate, when the maximum number of lithium atoms fills up all the adsorption sites of the graphene derivatives, and further addition of lithium atoms will result in strong Li–Li interaction rather with the carbon surface. Further, on probing the adsorption curve

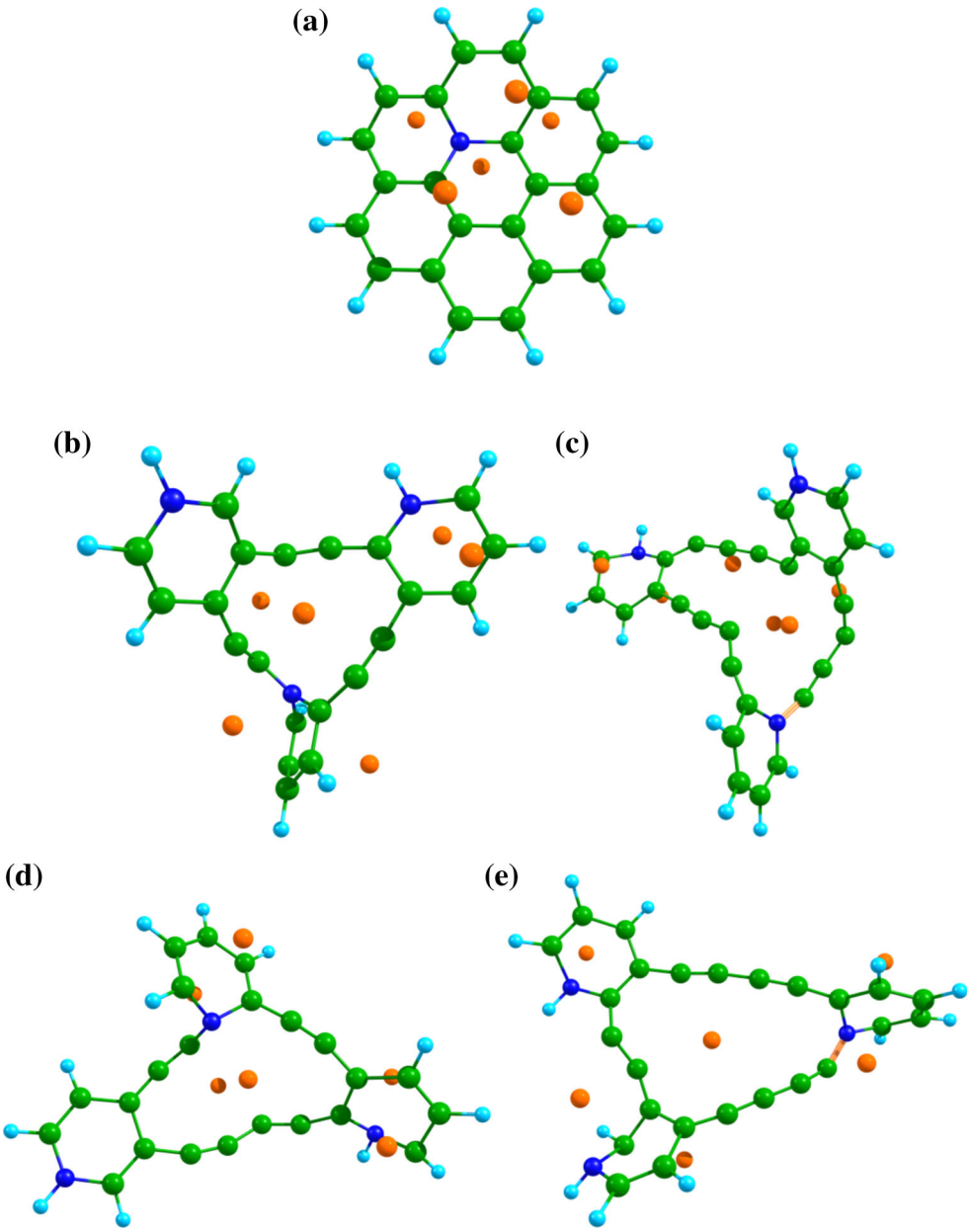

Figure 8 Optimized geometry of six lithium atoms adsorbed on nitrogen-doped **a** graphene, **b** graphyne, **c** graphdiyne, **d** G422, and **e** G442. *Orange balls* represent lithium atoms.

Table 3 Adsorption energy of Li on various sites of monolithiated graphene derivatives

Structures	Adsorption site					
	Bare structure		Boron doped		Nitrogen doped	
	Cavity site (eV)	Hexagonal site (eV)	Cavity site (eV)	Hexagonal site (eV)	Cavity site (eV)	Hexagonal site (eV)
GY	−1.72	−0.89	−3.57	−3.27	−1.72	−1.03
GDY	−1.45	−0.94	−2.82	−3.06	−1.96	−1.90
G422	−1.78	−0.85	−3.78	−3.25	−2.63	−0.53
G442	−1.86	−0.96	−3.51	−3.23	−2.19	−1.33

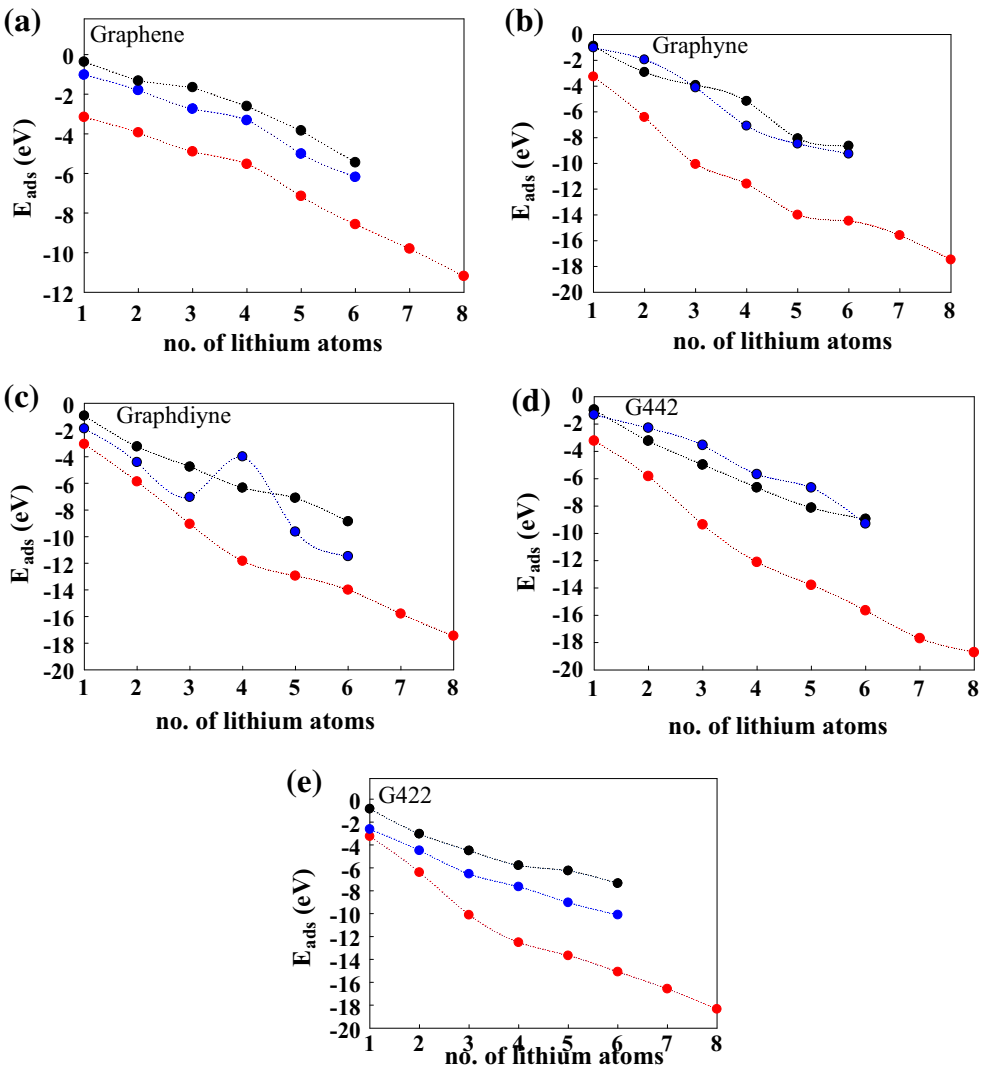

Figure 9 Variation of adsorption energy of lithium atom adsorbed on **a** graphene, **b** graphyne, **c** graphdiyne, **d** G442 and **e** G422 derivatives with respect to the number of lithium atoms adsorbed. *Black line* indicates bare graphene derivatives, *blue line* for nitrogen-doped and *red line* for boron-doped derivatives.

trend for the boronated derivatives, the curve saturates at four lithium atoms for graphene, whereas for the other derivatives the curve increases monotonously. This behavior of the curve indicates that the boronated graphene can hold only four lithium atoms, whereas the other structures can hold in excess of four lithium atoms. Likewise, nitrogen-doped graphene derivatives show better lithium adsorption affinity than bare graphene sheets even though the number of lithium atoms adsorbed is less compared to boron-doped structures. Thus, the above observation strongly supports that the doping of boron and nitrogen increases the lithium adsorption affinity in graphene and its derivatives. In general, the structures possessing more number of acetylenic linkages exhibits enhanced lithiation energy.

Further, the adsorption heights of the lithium atom on the lithiated complex are measured using the distance between the lithium atoms and the plane of the nanostructure and are listed in SI Table S2. The adsorption height varies with respect to the lithiation position on the nanostructure. The maximum height is observed for lithiation on hexagonal ring, whereas the least distance is at cavity position due to the absence of electron density. Besides, the range of adsorption height varies for each lithium atom, in which the adsorption height increases for the nitrogen-doped derivatives compared to the bare and boron-doped counterparts. Thus, similar to graphyne and graphdiyne, G442 and G422 structures also exhibit enhanced lithiation energy.

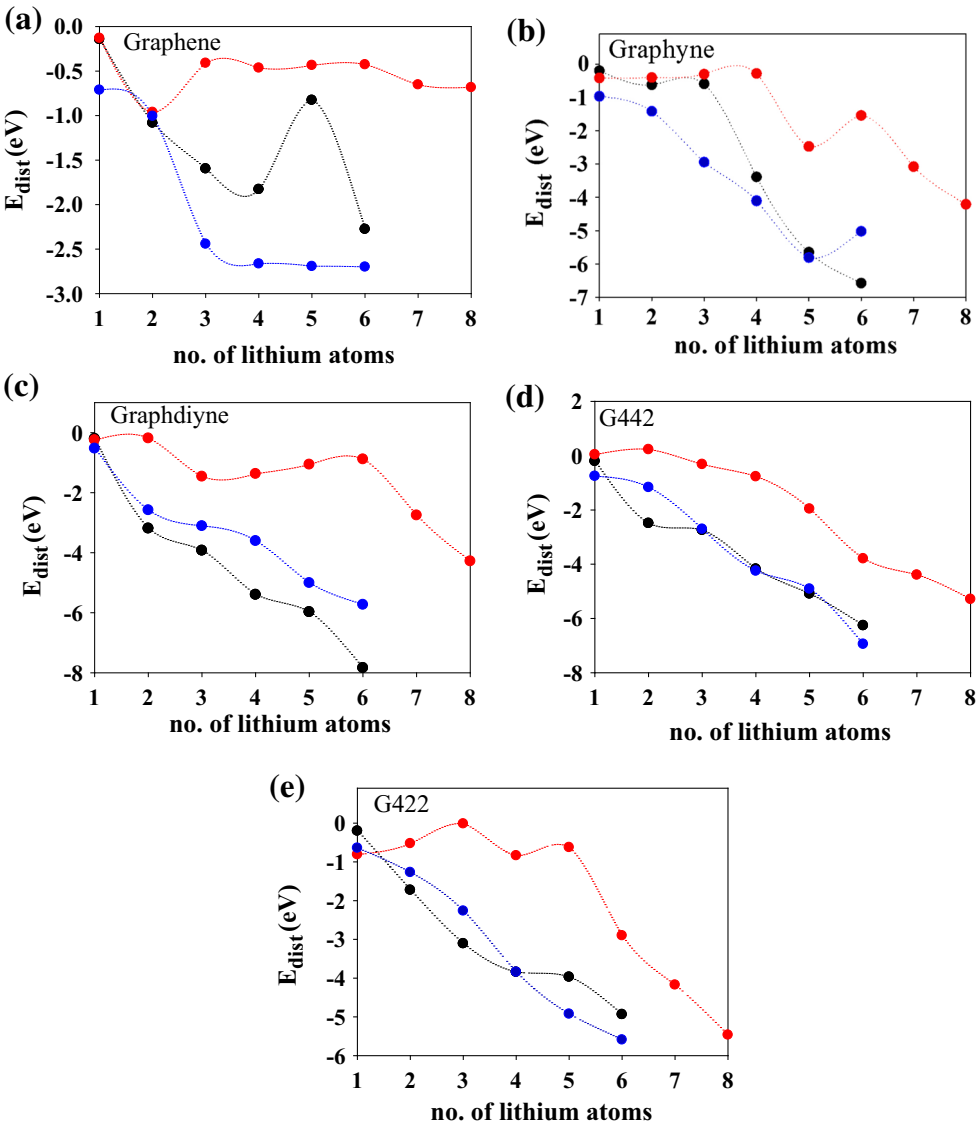

Figure 10 Variation of deformation energy created due to the adsorption of lithium atom on **a** graphene, **b** graphyne, **c** graphdiyne, **d** G442 and **e** G422 derivatives with respect to the number of lithium atoms adsorbed. *Black line* indicates bare graphene derivatives, *blue line* for nitrogen-doped and *red line* for boron-doped derivatives.

Deformation energy

Furthermore, the lithiation on the model compounds of the graphene derivatives leads to the deformation of the structures and is calculated using the relation, $E_{def} = E_{bare} - E_{distorted-Li}$, where E_{def} is the deformation energy (eV), E_{bare} is the energy of bare structure, and $E_{distorted-Li}$ is the energy of the distorted graphene derivatives in the lithium-loaded structure.

The deformation energy is estimated as the difference in the energies of bare graphene derivatives and that of the graphene derivatives in the lithiated complex.

The variation of deformation energy with respect to the number of lithium atoms adsorbed for the considered doped derivatives is plotted in Fig. 10. As the lithiation increases, both the bare and doped derivatives exhibit significant corrugations. The adsorption of lithium atoms leads to the structural deformation of the graphyne and graphdiyne derivatives in which the flat structure buckled in order to accommodate more lithium atoms. Interestingly, the boron-doped derivatives exhibit less structural deformations compared to the bare and nitrogen-doped derivatives, due to the presence of electron-deficient center in the boron-doped structures. The less deformation and the stability of a material are the deciding factors for the good anode materials, and the less-corrugated boron-doped counterparts offer a better hope for the anode materials. Finally, it is worth mentioning that the deformation of carbon structures due to lithiation is

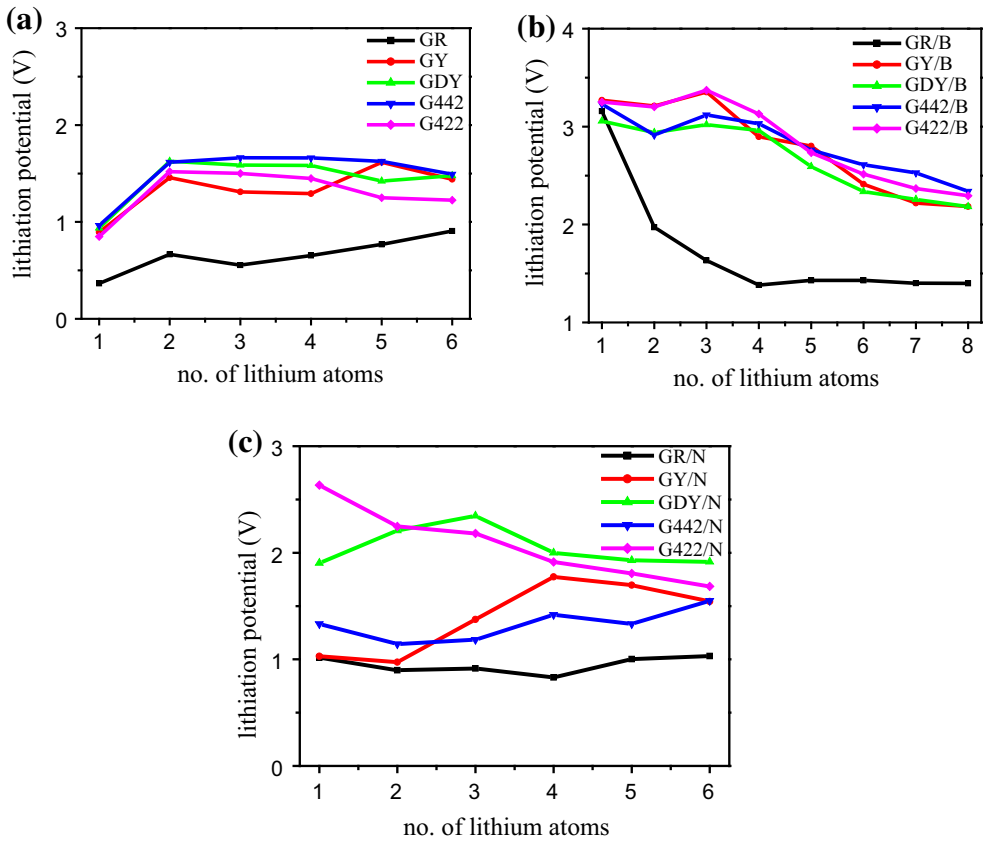

Figure 11 Variation of lithiation potential for **a** bare, **b** boron-, **c** nitrogen-doped derivatives.

minimized when the systems are considered periodic.

Lithiation potential and specific capacity

To verify the potential of these carbon nanostructures for the designation as an anode material for lithium batteries, we calculated the lithiation potential (using Eq. 3) and the specific capacities (using Eq. 4) for the bare and doped graphene derivatives, listed in SI Tables S3 and S4, respectively. The above-mentioned parameters for the eight-atom lithiated boron-doped derivatives are listed in SI Table S5. Graphical representation of the variation of lithiation potential with respect to the number of lithium atoms for bare structures and boron- and nitrogen-doped structures is shown in Fig. 11.

From Fig. 11, on increasing the number of lithium atoms, the lithiation potential decreases gradually in doped nanostructures. On the other hand, the range of the lithiation potential is considerably enhanced in boron doping, followed by nitrogen doping, when comparing with the bare structures. Among the bare structures, the six-atom lithiation potential is maximum for G442, which lies in the range of 0.964–1.493 V (on par with graphdiyne), and minimum for graphene (0.365–0.905 V). In the case of boron-doped derivatives, the improved lithiation potential is observed for graphyne (3.269–2.185 V) with eight lithium atoms, which is followed by G422/B, G442/B, and finally graphdiyne. Similarly, G422/N exhibits the improved lithiation potential of 2.634–1.685 V.

Generally, the lithiation potential of an anode material is inversely correlated with the specific capacity. That is, specific capacity increases with the decrease of lithiation potential values [31, 41]. Here the specific capacity curve (shown in Fig. 12) increases with respect to the number of lithium atoms in both bare and doped graphene derivatives. It is noted that the C_p values (Table S4) for both graphene and graphyne are exactly the same (470.01 mAh/g), as graphyne is an allotrope of graphene. Besides, the C_p values increase on boron doping and decrease on nitrogen doping. Among all the graphene derivatives possessing the acetylenic units, graphyne provides a

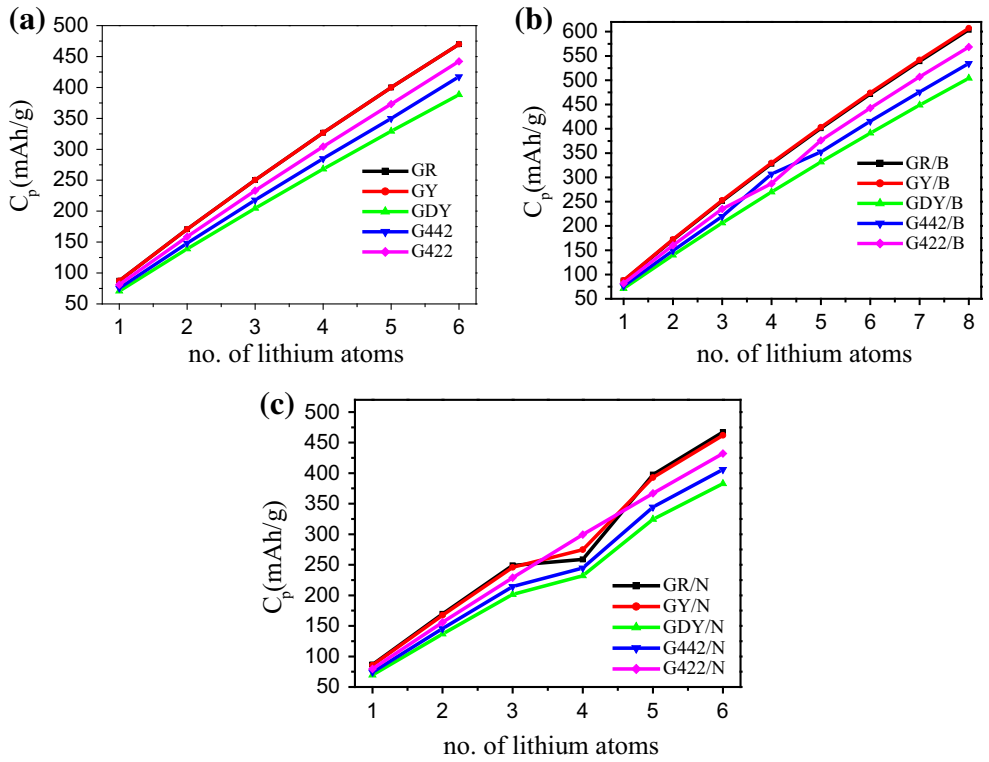

Figure 12 Variation of specific capacity for **a** bare, **b** boron-, **c** nitrogen-doped derivatives.

Table 4 Gravimetric density (%) of six-atom lithiated bare and nitrogen-doped derivatives and eight-atom lithiated boron-doped derivatives

Structures	Gravimetric density (%) (6 lithium atoms)	Structures	Gravimetric density (%) (8 lithium atoms)
GR	12.30	GR/B	15.80
GY	10.16		
GDY	12.30	GY/B	15.89
G442	10.79		
G422	11.50	GDY/B	13.20
GR/N	12.09		
GY/N	12.23	G442/B	13.99
GDY/N	10.02		
G442/N	10.62	G422/B	14.88
G422/N	11.31		

reasonable specific capacity of 470.01 mAh/g, whereas the others exhibit lower specific capacity values, and its boron counterpart exhibits 474.13 mAh/g for six-atom lithiation and 607.07 mAh/g for the loading of eight lithium atoms. These values are consistent with the specific capacity values of 623.4 and 788.4 mAh/g for graphyne and graphdiyne, respectively, reported for 3 × 3 × 1 supercell [27] in spite of being obtained from nonperiodic calculation. From the lithiation potential and specific capacity values, it can be demonstrated that the boron-doped graphyne, G442, and G422 structures exhibit reasonable performance as the anode material. Overall, the specific capacity values obtained from our models are better than that of graphite (364 mAh/g). If our model nanostructures are made periodic and then lithiated, the specific capacity will considerably improve.

Further, the gravimetric densities of the nanostructures are explored to estimate the maximum lithium adsorption capacity of the structure. The

gravimetric density (wt%) is calculated using Eq. 5 and listed in Table 4.

The gravimetric uptake of the nanostructures increases on boron doping, whereas it decreases with nitrogen doping. Among various boronated graphene model compounds, the boron-doped graphyne has the maximum value of wt% ~15.89 for the eight-atom lithiated complex and is also comparable with boron-doped graphene due to the equal number of carbon atoms. However, for the other model compounds like graphdiyne, G442/B, and G422/B, the slightly lower wt% values of 13.20, 13.99, and 14.88 %, respectively, are observed due to an increase in the number of carbon atoms. From the above-mentioned gravimetric densities, we see that boron-doped graphyne is an efficient lithium storage material and can possibly serve as a potential anode material in batteries. It is also worth to mention here that boronated graphene derivatives G442/G422 with varying acetylenic linkages can also be considered as alternative materials for efficient lithium storage.

Conclusion

In summary, the adsorption affinity for lithium is considerably higher in the graphene derivatives such as graphyne and graphdiyne than graphene. The varying number of acetylenic linkages exhibits improved lithium adsorption efficiency. Interestingly, on doping the electron-deficient boron atom, the adsorption affinity of lithium on the graphene derivatives increases, with less structural corrugations. From the lithiation potential and specific capacity values, it can be demonstrated that the boron-doped graphyne serves as a better anode material for lithium batteries. Moreover, structures with varying acetylenic units serve as a better alternative for both graphyne and graphdiyne.

Acknowledgements

One of the authors M. Lalitha acknowledges the financial support provided by Bharathiar University through University Research Fellowship (URF) (BU/Phy/URF-selection list/2013/398, dt. 08/05/2013). The authors are grateful to CMSD, University of Hyderabad, Hyderabad, India, for the use of computational resources high performance computing facility (HPCF).

Electronic supplementary material: The online version of this article (doi:10.1007/s10853-016-0378-6) contains supplementary material, which is available to authorized users.

References

[1] Ibrahim H, Ilinca A, Perron J (2008) Energy storage systems—characteristics and comparisons. Renew Sustain Energy Rev 12(5):1221–1250. doi:10.1016/j.rser.2007.01.023

[2] Simon P, Gogotsi Y (2008) Materials for electrochemical capacitors. Nat Mater 7(11):845–854. doi:10.1038/nmat2297

[3] Kim JG, Son B, Mukherjee S, Schuppert N, Bates A, Kwon O, Choi MJ, Chung HY, Park S (2015) A review of lithium and non-lithium based solid state batteries. J Power Sources 282:299–322. doi:10.1016/j.jpowsour.2015.02.054

[4] Scrosati B, Garche J (2010) Lithium batteries: status, prospects and future. J Power Sources 195(9):2419–2430. doi:10.1016/j.jpowsour.2009.11.048

[5] van Schalkwijk W, Scrosati B (2004) Advances in lithium–ion batteries. KluwerAcademic/Plenum, Boston

[6] Whittingham MS (2004) Lithium batteries and cathode materials. Chem Rev 104(10):4271–4302. doi:10.1021/cr020731c

[7] Kang B, Ceder G (2009) Battery materials for ultrafast charging and discharging. Nature 458(7235):190–193. doi:10.1038/nature07853

[8] Wang Y, Cao G (2008) Developments in nanostructured cathode materials for high-performance lithium–ion batteries. Adv Mater 20(12):2251–2269. doi:10.1002/adma.200702242

[9] Ellis BL, Lee KT, Nazar LF (2010) Positive electrode materials for Li–ion and Li-batteries. Chem Mater 22(3):691–714. doi:10.1021/cm902696j

[10] Wang S, Li S, Sun Y, Feng X, Chen C (2011) Three-dimensional porous V_2O_5 cathode with ultra high rate capability. Energy Environ Sci 4(8):2854–2857. doi:10.1039/c1ee01172c

[11] Stournara ME, Guduru PR, Shenoy VB (2012) Elastic behavior of crystalline Li–Sn phases with increasing Li concentration. J Power Sources 208:165–169. doi:10.1016/j.jpowsour.2012.02.022

[12] Miller JR, Simon P (2008) Electrochemical capacitors for energy management. Science 321(5889):651–652. doi:10.1126/science.1158736

[13] Esmanski A, Ozin GA (2009) Silicon inverse-opal-based macroporous materials as negative electrodes for lithium ion batteries. Adv Funct Mater 19(12):1999–2010. doi:10.1002/adfm.200900306

[14] Garay-Tapia AM, Romero AH, Barone V (2012) Lithium adsorption on graphene: from isolated adatoms to metallic sheets. J Chem Theory Comput 8(3):1064–1071. doi:10.1021/ct300042p

[15] Sun Q, Jena P, Wang Q, Marquez M (2006) First-principles study of hydrogen storage on Li12C60. J Am Chem Soc 128(30):9741–9745. doi:10.1021/ja058330c

[16] Yoo E, Kim J, Hosono E, Zhou H-S, Kudo T, Honma I (2008) Large reversible Li storage of graphene nanosheet families for use in rechargeable lithium ion batteries. Nano Lett 8(8):2277–2282. doi:10.1021/nl800957b

[17] Lee SW, Gallant BM, Byon HR, Hammond PT, Shao-Horn Y (2011) Nanostructured carbon-based electrodes: bridging the gap between thin-film lithium–ion batteries and electrochemical capacitors. Energy Environ Sci 4(6):1972–1985. doi:10.1039/c0ee00642d

[18] Zhao Y, Kim Y-H, Dillon AC, Heben MJ, Zhang SB (2005) Hydrogen storage in novel organometallic buckyballs. Phys Rev Lett 94(15):155504. doi:10.1103/PhysRevLett.94.155504

[19] Phillips AB, Shivaram BS (2008) High capacity hydrogen absorption in transition metal–ethylene complexes observed via nanogravimetry. Phys Rev Lett 100(10):105505. doi:10.1103/PhysRevLett.100.105505

[20] Sun Q, Wang Q, Jena P, Kawazoe Y (2005) Clustering of Ti on a C60 surface and its effect on hydrogen storage. J Am Chem Soc 127(42):14582–14583. doi:10.1021/ja0550125

[21] Han SS, Goddard WA (2007) Lithium-doped metal-organic frameworks for reversible H_2 storage at ambient temperature. J Am Chem Soc 129(27):8422–8423. doi:10.1021/ja072599+

[22] Lan J, Cao D, Wang W (2009) Li12Si60H60 fullerene composite: a promising hydrogen storage medium. ACS Nano 3(10):3294–3300. doi:10.1021/nn900842j

[23] Geim AK, Novoselov KS (2007) The rise of graphene. Nat Mater 6(3):183–191. doi:10.1038/nmat1849

[24] Novoselov KS, Geim AK, Morozov SV, Jiang D, Katsnelson MI, Grigorieva IV, Dubonos SV, Firsov AA (2005) Two-dimensional gas of massless Dirac fermions in graphene. Nature 438(7065):197–200. doi:10.1038/nature04233

[25] Novoselov KS, Jiang Z, Zhang Y, Morozov SV, Stormer HL, Zeitler U, Maan JC, Boebinger GS, Kim P, Geim AK (2007) Room-temperature quantum hall effect in graphene. Science 315(5817):1379–1379. doi:10.1126/science.1137201

[26] Murugesan V, Hu J (2013) Exploring the interaction between lithium ion and defective graphene surface using dispersion corrected DFT studies. ECS Trans 53(10):23–32. doi:10.1149/05310.0023ecst

[27] Schlapbach L, Zuttel A (2001) Hydrogen-storage materials for mobile applications. Nature 414(6861):353–358. doi:10.1038/35104634

[28] Winter M, Besenhard JO, Spahr ME, Novák P (1998) Insertion electrode materials for rechargeable lithium batteries. Adv Mater 10(10):725–763. doi:10.1002/(sici)1521-4095(199807)10:10<725:aid-adma725>3.0.co;2-z

[29] Kaskhedikar NA, Maier J (2009) Lithium storage in carbon nanostructures. Adv Mater 21(25–26):2664–2680. doi:10.1002/adma.200901079

[30] Profeta G, Calandra M, Mauri F (2012) Phonon-mediated superconductivity in graphene by lithium deposition. Nat Phys 8(2):131–134. doi:10.1038/nphys2181

[31] Srinivasu K, Ghosh SK (2012) Graphyne and graphdiyne: promising materials for nanoelectronics and energy storage applications. J Phys Chem C 116(9):5951–5956. doi:10.1021/jp212181h

[32] Sun C, Searles DJ (2012) Lithium storage on graphdiyne predicted by DFT calculations. J Phys Chem C 116(50):26222–26226. doi:10.1021/jp309638z

[33] Zhang H, Zhao M, He X, Wang Z, Zhang X, Liu X (2011) High mobility and high storage capacity of lithium in sp–sp^2 hybridized carbon network: the case of graphyne. J Phys Chem C 115(17):8845–8850. doi:10.1021/jp201062m

[34] Chandra Shekar S, Swathi RS (2013) Rattling motion of alkali metal ions through the cavities of model compounds of graphyne and graphdiyne. J Phys Chem A 117(36):8632–8641. doi:10.1021/jp402896v

[35] Wang H, Zhang C, Liu Z, Wang L, Han P, Xu H, Zhang K, Dong S, Yao J, Cui G (2011) Nitrogen-doped graphene nanosheets with excellent lithium storage properties. J Mater Chem 21(14):5430–5434. doi:10.1039/c1jm00049g

[36] Yu Y-X (2013) Can all nitrogen-doped defects improve the performance of graphene anode materials for lithium–ion batteries? Phys Chem Chem Phys 15(39):16819–16827. doi:10.1039/c3cp51689j

[37] Ma C, Shao X, Cao D (2012) Nitrogen-doped graphene nanosheets as anode materials for lithium ion batteries: a first-principles study. J Mater Chem 22(18):8911–8915. doi:10.1039/c2jm00166g

[38] Mukhopadhyay I, Hoshino N, Kawasaki S, Okino F, Hsu WK, Touhara H (2002) Electrochemical Li insertion in B-doped multiwall carbon nanotubes. J Electrochem Soc 149(1):A39–A44

[39] Zhou Z, Zhao J, Gao X, Chen Z, Yan J, von Ragué Schleyer P, Morinaga M (2005) Do composite single-walled nanotubes have enhanced capability for lithium storage? Chem Mater 17(5):992–1000. doi:10.1021/cm048746+

[40] Lu R, Rao D, Meng Z, Zhang X, Xu G, Liu Y, Kan E, Xiao C, Deng K (2013) Boron-substituted graphyne as a versatile

material with high storage capacities of Li and H2: a multiscale theoretical study. Phys Chem Chem Phys 15(38):16120–16126. doi:10.1039/c3cp52364k

[41] Aydinol MK, Kohan AF, Ceder G, Cho K, Joannopoulos J (1997) Ab initio study of lithium intercalation in metal oxides and metal dichalcogenides. Phys Rev B 56(3):1354–1365. doi:10.1103/PhysRevB.56.1354

[42] Chai J-D, Head-Gordon M (2008) Long-range corrected hybrid density functionals with damped atom-atom dispersion corrections. Phys Chem Chem Phys 10(44):6615–6620. doi:10.1039/b810189b

[43] Umadevi D, Sastry GN (2011) Quantum mechanical study of physisorption of nucleobases on carbon materials: graphene versus carbon nanotubes. J Phys Chem Lett 2(13):1572–1576. doi:10.1021/jz200705w

[44] Maroulis G (1999) On the accurate theoretical determination of the static hyperpolarizability of trans-butadiene. J Chem Phys 111(2):583–591. doi:10.1063/1.479339

[45] Maroulis G, Xenides D, Hohm U, Loose A (2001) Dipole, dipole–quadrupole, and dipole–octopole polarizability of adamantane, C10H16, from refractive index measurements, depolarized collision-induced light scattering, conventional ab initio and density functional theory calculations. J Chem Phys 115(17):7957–7967. doi:10.1063/1.1410392

[46] Karamanis P, Maroulis G (2011) An ab initio study of CX3-substitution (X = H, F, Cl, Br, I) effects on the static electric polarizability and hyperpolarizability of diacetylene. J Phys Org Chem 24(7):588–599. doi:10.1002/poc.1797

[47] Karamanis P, Maroulis G (2003) Single (C–C) and triple (C–C) bond-length dependence of the static electric polarizability and hyperpolarizability of H-C–C–C–C–H. Chem Phys Lett 376(3–4):403–410. doi:10.1016/S0009-2614(03)00784-X

[48] Frisch MJ, Trucks GW, Schlegel HB, Scuseria GE, Robb MA, Cheeseman JR, Scalmani G, Barone V, Mennucci B, Petersson GA, Nakatsuji H, Caricato M, Li X, Hratchian HP, Izmaylov AF, Bloino J, Zheng G, Sonnenberg JL, Hada M, Ehara M, Toyota K, Fukuda R, Hasegawa J, Ishida M, Nakajima T, Honda Y, Kitao O, Nakai H, Vreven T, Montgomery JA Jr, Peralta JE, Ogliaro F, Bearpark MJ, Heyd J, Brothers EN, Kudin KN, Staroverov VN, Kobayashi R, Normand J, Raghavachari K, Rendell AP, Burant JC, Iyengar SS, Tomasi J, Cossi M, Rega N, Millam NJ, Klene M, Knox JE, Cross JB, Bakken V, Adamo C, Jaramillo J, Gomperts R, Stratmann RE, Yazyev O, Austin AJ, Cammi R, Pomelli C, Ochterski JW, Martin RL, Morokuma K, Zakrzewski VG, Voth GA, Salvador P, Dannenberg JJ, Dapprich S, Daniels AD, Farkas Ö, Foresman JB, Ortiz JV, Cioslowski J, Fox DJ (2009) Gaussian 09. Gaussian Inc, Wallingford

[49] Fonseca Guerra C, Snijders GJ, te Velde G, Baerends JE (1998) Towards an order-N DFT method. Theoret Chem Acc 99(6):391–403. doi:10.1007/s002140050353

[50] te Velde G, Bickelhaupt FM, Baerends EJ, Fonseca Guerra C, van Gisbergen SJA, Snijders JG, Ziegler T (2001) Chemistry with ADF. J Comput Chem 22(9):931–967. doi:10.1002/jcc.1056

[51] Jiao Y, Du A, Hankel M, Zhu Z, Rudolph V, Smith SC (2011) Graphdiyne: a versatile nanomaterial for electronics and hydrogen purification. Chem Commun 47(43):11843–11845. doi:10.1039/c1cc15129k

[52] Lazar P, Zboril R, Pumera M, Otyepka M (2014) Chemical nature of boron and nitrogen dopant atoms in graphene strongly influences its electronic properties. Phys Chem Chem Phys 16(27):14231–14235. doi:10.1039/c4cp01638f

[53] Lu T, Chen F (2012) Multiwfn: a multifunctional wavefunction analyzer. J Comput Chem 33(5):580–592. doi:10.1002/jcc.22885

[54] Murray JS, Politzer P (2011) The electrostatic potential: an overview. Wiley Interdiscip Rev Comput Mol Sci 1(2):153–163. doi:10.1002/wcms.19

[55] Umadevi V, Mano Priya A, Senthilkumar L (2015) DFT study on the tautomerism of organic linker 1H-imidazole-4,5-tetrazole (HIT). Comput Theor Chem 1068:149–159. doi:10.1016/j.comptc.2015.06.022

[56] Ferre-Vilaplana A (2008) Storage of hydrogen adsorbed on alkali metal doped single-layer all-carbon materials. J Phys Chem C 112(10):3998–4004. doi:10.1021/jp0768874